RESEARCH ARTICLE | JUNE 05 2023

Effect of Nd doping on the crystallographic, magnetic, and magnetocaloric properties of $Nd_xGd_{3-x}CoNi$

A. Oleaga ✉; A. Erkoreka; A. Herrero; ... et. al

APL Mater 11, 061112 (2023)
https://doi.org/10.1063/5.0153045

Effect of Nd doping on the crystallographic, magnetic, and magnetocaloric properties of $Nd_xGd_{3-x}CoNi$

Cite as: APL Mater. 11, 061112 (2023); doi: 10.1063/5.0153045
Submitted: 4 April 2023 • Accepted: 18 May 2023 •
Published Online: 5 June 2023

A. Oleaga,[1,a] A. Erkoreka,[1] A. Herrero,[1] A. Provino,[2] D. Peddis,[2,3] and P. Manfrinetti[2,4]

AFFILIATIONS

[1] Departamento de Física Aplicada, Escuela de Ingeniería de Bilbao, Universidad del País Vasco UPV/EHU, Plaza Ingeniero Torres Quevedo 1, 48013 Bilbao, Spain
[2] Department of Chemistry, University of Genova, Via Dodecaneso 31, Genova 16146, Italy
[3] Institute of Structure of Matter (ISM) - CNR (nM2-Lab), Via Salaria, Monterotondo Scalo, 00015 Rome, Italy
[4] Institute SPIN – CNR, Corso Perrone 24, 16152 Genova, Italy

[a] **Author to whom correspondence should be addressed:** alberto.oleaga@ehu.es

ABSTRACT

The crystal structure, magnetic and magnetocaloric properties, and the critical behavior of representative compounds in the pseudo-ternary $Nd_xGd_{3-x}CoNi$ series have been investigated (x = 0.15, 0.5, 1.0, and 1.5). All these phases are isotypic with the parent compound Gd_3CoNi, crystallizing with the monoclinic Dy_3Ni_2-type (*mS*20, *C*2/*m*, No. 12). All samples present a paramagnetic to ferromagnetic (PM-FM) second order phase transition with decreasing Curie temperature as the Nd concentration is increased (T_C = 171, 150, 120, and 96 K, respectively) and, at lower temperatures, there is a spin reorientation, which leads to a complex magnetic ground state. The critical exponents (β, γ, and δ) have been retrieved for the PM-FM transitions. On the one hand, in x = 0.15, 0.5, and 1.5 the value of $\gamma \approx 1$ indicates that the magnetic interactions are long-range order while the values of β point to a certain deviation from the 3D-Heisenberg universality class; on the other hand, $NdGd_2CoNi$ has a particular critical behavior, as β is close to the mean field model while γ is close to the uniaxial 3D-Ising one. Concerning the magnetocaloric properties, the magnetic entropy change and refrigerant capacity present competitive values, interesting for cryogenic applications. Finally, the thermal diffusivity values of these compounds are extremely good for practical magnetocaloric refrigeration systems, as they are in the range 1.5–3 mm^2/s.

I. INTRODUCTION

The development of magnetocaloric refrigeration as an alternative to the gas compression–expansion cycles refrigerators is being the subject of a huge number of papers and reviews in the last decade. Different kinds of materials have been studied looking for optimal magnetocaloric properties: Heusler alloys, rare-earth based intermetallic materials, rare-earth free materials, High Entropy Alloys, composites, etc.[1–10] Materials with first order magnetic phase transitions give, in general, a higher magnetic entropy change but the hysteresis prevents them from being used in practical prototypes due to a gross efficiency reduction when working along a cycle. Thus, though first order phase transitions with negligible hysteresis are being looked for, there is also a great interest in magnetocaloric effects related to second order phase transitions with relevant properties whose absence of hysteresis makes them useful. The aim to have them working in refrigeration cycles makes it extremely relevant to also look into how fast heat is transported within the material and exchanged with the environment. In this sense, intermetallic materials have, in general, better properties than other families of materials. Finally, though room temperature refrigeration is extremely important, there is also a growing focus on finding magnetocaloric materials, which can work in other temperature ranges, such as the gas liquefaction ones. In order to be able to tune the

temperature application range, families of rare-earth based intermetallic materials, where doping is introduced or rare-earths are combined, are promising candidates for different refrigeration applications.

The few studies performed on the particular family of ternary intermetallics R_3CoNi (R = Gd, Tb, Dy, Ho, Er, and Tm)[11–13] have shown that they present relevant magnetocaloric properties from very low temperature to 170 K (the latter being the case of Gd_3CoNi). The aim of this work is to study how the addition of Nd changes these properties and if at some composition they might be remarkable. Therefore, a complete study on the crystallographic, magnetic, magnetocaloric, and thermal properties of Nd_xGd_{3-x}CoNi (x = 0.15, 0.5, 1.0, and 1.5) has been undertaken. It will include a critical behavior study of the paramagnetic to ferromagnetic (PM-FM) phase transition, as this gives a further insight on the magnetic and magnetocaloric properties of the compounds.

II. SAMPLES SYNTHESIS AND CHARACTERIZATION, EXPERIMENTAL TECHNIQUES

A. Samples synthesis and phase analysis

Samples with nominal composition Nd_xGd_{3-x}CoNi (x = 0, 0.15, 0.5, 1.0, and 1.5) were synthesized by arc melting pieces of metallic elements, weighed in the stoichiometric proportion and under a TiZr-gettered Ar atmosphere. The starting constituents were commercial high purity metals: Nd and Gd (both 99.9 wt. % purity), Co and Ni (both 99.99 wt. % purity); total amount of about 3 g. The buttons were melted three-four times, turning them upside down after each melting to ensure homogenization; weight loss was between 0.2 and 0.4 wt. %. The obtained ingots were wrapped in a Ta foil, sealed under vacuum in SiO_2 tubes, and annealed at temperatures between 700 and 750 °C for 7 days; the alloys were then slowly cooled down to room temperature after turning off the power to the furnace.

The homogeneity of samples and their microstructure were checked by light optical microscopy (LOM) and scanning electron microscopy (SEM) complemented with a semiquantitative microprobe [energy dispersive x ray (EDX)] [Leica Cambridge 360 microscope, equipped with an Oxford X-Max 20 analyzer. Work parameters: EHT 20.0 kV and probe current 220 pA (Oxford Aztec software)]. The micrographic specimens were prepared by standard polishing technique using SiC abrasive papers, down to 1 μm by diamond paste, of a section of samples (cut vertically from top to bottom). Pure Co and a sample of the parent Gd_3CoNi were used as reference standard materials; in this way, the accuracy of the EDX measurements was estimated to be within 0.6 at. %. For all samples, the chemical composition measured on the total area of the specimens (15–20 mm^2) resulted in very good agreement with the nominal one.

The crystal structure of the phases was investigated by powder x-ray diffraction (XRD). The powder patterns were collected by using a Bruker D4-Endeavour diffractometer for data collection (Cu Kα radiation, with 2θ range of 5°–100°). Pure Si was used as an external standard, a = 5.4308(1) Å. The patterns were indexed by the help of Lazy Pulverix;[14] accurate lattice parameters were calculated by means of least-square methods (handmade software). Rietveld structural refinements were carried out by using the FullProf software.[15]

B. Physical properties measurements

Magnetic measurements have been performed using a Vibrating Sample Magnetometer by Cryogenic Limited, in order to obtain the Zero-Field Cooled (ZFC), Field-Cooled (FC) magnetization curves (with applied field $\mu_0 H$ = 100 Oe) from 2 to 300 K. Once the magnetic transitions have been located, the magnetization (M) of the samples under external applied magnetic fields H_a in the range of 0–7 T has been measured. For all samples, isotherms have been collected from 2 K to temperatures well above the corresponding Curie temperature (T_C), using different steps, depending on the temperature range. As there might be metamagnetic transitions or other first order phase transitions at low temperature, a discontinuous procedure has been used to measure them, so that the Maxwell equation can be used to obtain the magnetic entropy change. In order to study in detail the critical behavior of the paramagnetic-ferromagnetic transition, a step of ΔT = 1 K has been taken between consecutive isotherms around T_C; additionally, demagnetization effects have been considered to perform a correct evaluation of the magnetocaloric effect and the scaling analysis.[3,16] For this purpose, the demagnetization factor N has been obtained by means of *ac* susceptibility measurements,[17,18] and the internal magnetic field has afterward been calculated using the equation $H_i = H_a - NM$. In order to maintain a notation as simple as possible throughout the paper, H will be used instead of H_i to represent the internal field. The magnetic susceptibility has been measured with the AC Measurement System Option in a Physical Properties Measurement System (PPMS) by Quantum Design, for a frequency f = 100 Hz. The values of N are 29.43 gOe/emu for $Nd_{0.15}Gd_{2.85}$CoNi, 48.49 gOe/emu for $Nd_{0.5}Gd_{2.5}$CoNi, 98.43 gOe/emu for $NdGd_2$CoNi and 101.20 gOe/emu for $Nd_{1.5}Gd_{1.5}$CoNi.

Regarding thermal properties, the thermal diffusivity has been measured by means of a high resolution *ac* photopyroelectric calorimeter in the back detection configuration.[19]

III. EXPERIMENTAL RESULTS AND DISCUSSION

A. Crystallographic studies/characterization

Samples with nominal composition Nd_xGd_{3-x}CoNi (x = 0, 0.15, 0.5, 1.0, and 1.5) were prepared. Gd_3CoNi is presented here to visualize the evolution of the crystalline properties with Nd doping but, as its magnetic and magnetocaloric properties have already been studied,[11] it is excluded from the rest of the study. X-ray powder diffraction and SEM-EDX analyses were carried out on each sample. All samples contain a small percentage of the pseudo-binary equiatomic secondary phase $(NdGd)_1(CoNi)_1$ (between about 1% for the sample with x = 0.15, to about 4%–5% with x = 1.5). Figure S1, in the supplementary material, shows selected SEM microphotographs (backscattered electrons) as representative examples of some samples; the extra phase showing up as small darker grains. Table I collects the lattice parameters (a, b, c, and β) and unit cell volume (V_{cell}) for the Nd_xGd_{3-x}CoNi phase (monoclinic Dy_3Ni_2-type, $mS20$, $C2/m$, No. 12) contained in the different samples. Table II reports the data of the Rietveld refinement obtained for the sample with nominal composition $Nd_{1.5}Gd_{1.5}$CoNi. Figure 1 shows the trend of the lattice parameters (a, b, c, and β) and unit cell volume (V_{cell}) for the Nd_xGd_{3-x}CoNi (monoclinic Dy_3Ni_2-type, $mS20$, $C2/m$, No. 12) series as a function of the Nd content, x. Nd doping

TABLE I. Lattice parameters (*a*, *b*, *c*, and *β*) and unit cell volume (V_{cell}) for the $Nd_xGd_{3-x}CoNi$ phase (monoclinic Dy_3Ni_2-type, *mS*20, *C*2/*m*, No. 12) contained in the samples prepared with nominal composition $Nd_xGd_{3-x}CoNi$ with x = 0, 0.15, 0.5, 1.0, and 1.5.

	Crystallographic data				
Nominal composition	*a* (Å)	*b* (Å)	*c* (Å)	*β* (°)	V_{cell} (Å^3)
Gd_3CoNi	13.407(2)	3.8118(7)	9.535(2)	109.08(1)	460.52(9)
$Nd_{0.15}Gd_{2.85}CoNi$	13.414(1)	3.8111(3)	9.5486(8)	108.96(5)	461.66(7)
$Nd_{0.5}Gd_{2.5}CoNi$	13.435(1)	3.8156(4)	9.5712(9)	108.96(2)	464.05(8)
$NdGd_2CoNi$	13.465(2)	3.8173(5)	9.6041(7)	108.88(3)	467.07(9)
$Nd_{1.5}Gd_{1.5}CoNi$	13.504(1)	3.8208(1)	9.6417(2)	108.75(2)	471.09(2)

leads to an isotropic increase of the three lattice parameters *a*, *b*, *c*, and to a decrease of parameter *β*. The overall result is an increase of the Unit-cell volume, as expected based on a larger atomic volume of Nd compared with that of Gd.[20] Figures 2 and 3 show the Rietveld refinement profile for the samples $Nd_{1.5}Gd_{1.5}CoNi$ and $Nd_{0.5}Gd_{2.5}CoNi$, respectively.

B. Magnetic properties

The magnetization as a function of temperature is shown in Fig. 4(a) for the four compositions, both in Zero-Field Cooled (ZFC) and Field-Cooled (FC), with an applied field of 100 Oe; meanwhile, Fig. 4(b) contains the real part of the *ac* susceptibility, which is very sensitive to accurately find the critical temperature of any phase transition; nevertheless, as in some cases, the peak is not well marked, the first derivative of the magnetization has also been used to locate T_C. The addition of Nd has several effects when compared with the parent compound Gd_3CoNi, where a paramagnetic to ferromagnetic second order phase transition takes place at 170 K and the ZFC and FC curves perfectly superimpose in the whole temperature range.[11] The Curie temperature (T_C) of the paramagnetic to ferromagnetic phase transition is reduced as Nd concentration is increased (T_C = 171, 150, 120, and 96 K for x = 0.15, 0.5, 1, and 1.5, respectively), maintaining the second order character (this has been confirmed by the thermal measurements later shown). The ZFC and FC curves separate further one from another as x is raised, indicating the introduction of thermomagnetic irreversibility, which is typical of many ferro/ferrimagnetic transitions, including the other members of the R_3CoNi family (*R* = Tb, Dy, Ho, Er, and Tm) already studied.[13] Only in the case of Gd_3CoNi this effect does not take place.[11]

Around 50 K (but with a small drift to a lower temperature as Nd concentration is increased) a peak in the real part of the *ac* susceptibility emerges, which corresponds to a bump in the magnetization, for the four compounds. This is due to a certain spin reorientation to a complex magnetic ground state, as the magnetization isotherms will show later. Similar transitions appear in other members of the R_3CoNi family.[13]

TABLE II. Rietveld refinement data obtained for the sample with nominal composition $Nd_{1.5}Gd_{1.5}CoNi$ (R_{wp} = 10.5%, χ^2 = 1.16). The sample contains: 95.3(8)% of the monoclinic Dy_3Ni_2-type $Nd_{1.51(3)}Gd_{1.49(3)}CoNi$ compound and 4.7(3)% of the orthorhombic CrB-type $Nd_{0.40}Gd_{0.60}Co_{0.40}Ni_{0.60}$ phase. (*) the starting Nd/Gd occupancy in each one of the three 4*i* sites has been set as 50: 50, then it has been refined by constraining the same value for all three sites.

Atom	Wyckoff site	*x*	*y*	*z*	Occ.	B_{iso} (Å^2)
Nd_1/Gd	4*i*	0.3716(3)	0	0.0039(3)	0.57/0.43(1)*	2.90(1)
Nd_2/Gd	4*i*	0.0989(2)	0	0.6682(3)	0.57/0.43(1)*	2.84(1)
Nd_3/Gd	4*i*	0.3617(2)	0	0.6267(3)	0.57/0.43(1)*	2.75(1)
Co	4*i*	0.2218(6)	0	0.2265(6)	1	2.87(2)
Ni	4*i*	0.0139(6)	0	0.1160(6)	1	2.84(2)

Phase 1: $Nd_{1.51(3)}Gd_{1.49(3)}CoNi$ (final refined composition) Dy_3Ni_2-type (*mS*20, *C*2/*m*, No. 12) [95.3(8) %]
R_B = 0.68%, R_F = 0.96%
Lattice parameters: *a* = 13.5042(4) Å, *b* = 3.8208(1) Å, *c* = 9.6417(2) Å, *β* = 108.748(1)°
V_{cell} = 471.09(2) Å^3
Phase 2: $Nd_{0.40}Gd_{0.60}Co_{0.40}Ni_{0.60}$ (composition as from SEM-EDX; not refined) [4.7(3) %].
CrB-type (*oS*8, *Cmcm*, No. 63)
R_B = 1.38%, R_F = 1.35%; B_{over} = 0.15(6) Å^2
Lattice parameters: *a* = 3.9284(5), *b* = 10.935(2) Å, *c* = 3.9980(5) Å, V_{cell} = 171.74(4) Å^3.

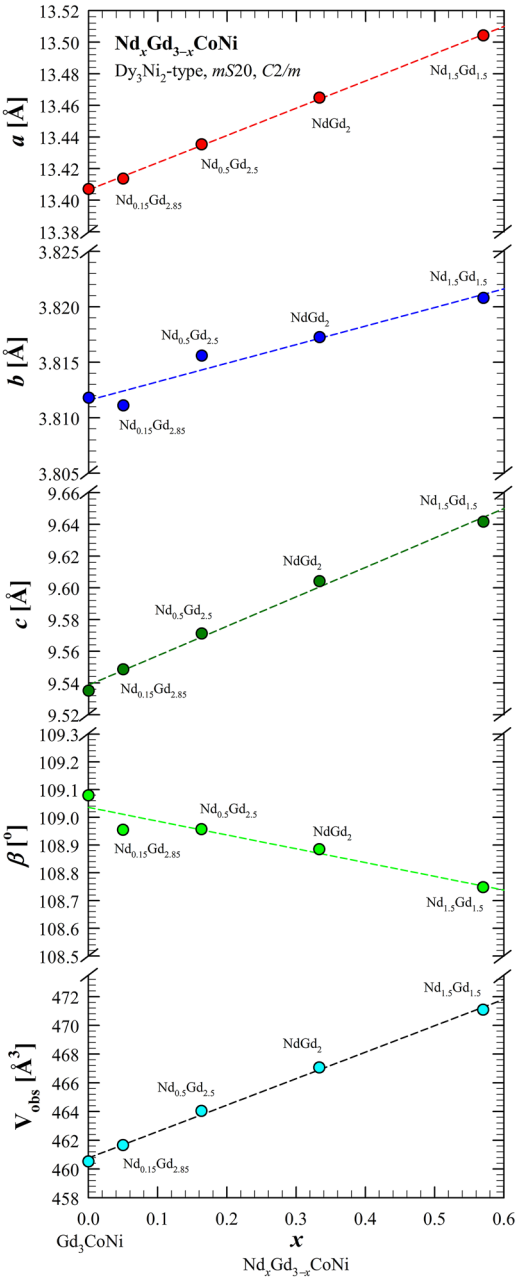

FIG. 1. Trend of the lattice parameters (*a*, *b*, *c* and *β*) and unit cell volume (V_{cell}) for the $Nd_xGd_{3-x}CoNi$ phase (monoclinic Dy_3Ni_2-type, *mS*20, *C*2/*m*, No. 12) as a function of the Nd content, x, in the samples prepared with nominal composition $Nd_xGd_{3-x}CoNi$, with x = 0, 0.15, 0.5, 1.0, and 1.5.

Finally, in the *ac* susceptibility of $Nd_{0.5}Gd_{2.5}CoNi$ and $NdGd_2CoNi$ a small peak can be seen at 109, 100 K, respectively, while there is only a small shoulder in $Nd_{1.5}Gd_{1.5}CoNi$ at 89 K [see the arrows in Fig. 4(b)]. The two latter transitions can also be observed in the magnetization curves [Fig. 4(a)], whereas all these features appear at the same temperatures in the thermal diffusivity curves shown in the Sec. III E, as well. This implies that at those temperatures the orientation of the spins is already evolving.

The evolution of the thermomagnetic irreversibility with Nd concentration is confirmed by the hysteresis loops at 2 K, which are shown in Fig. 5. The sample with less Nd contents (x = 0.15) presents no measurable coercive field, while there is a growing one as x is increased ($\mu_0 H_c$ = 0.023 T for x = 0.5, $\mu_0 H_c$ = 0.08 T for x = 1, and $\mu_0 H_c$ = 0.168 T for x = 1.5). There are no clear metamagnetic transitions as it happens in Tb_3CoNi[13] but there are some distinct features at about 1.5 T in $Nd_{0.5}Gd_{2.5}CoNi$ and close to 2 T in $NdGd_2CoNi$, suggesting particular magnetic behaviors. These will be clear when presenting the magnetization isotherms at low temperature as a function of the field later in this section.

As it has been already mentioned, Gd_3CoNi does not present any kind of thermomagnetic irreversibility, it is the introduction of Nd that provokes it. This is a phenomenon found in ferromagnetic materials with magnetocrystalline anisotropies, materials with competing magnetic interactions, and spin glasses.[21–23] The presence of coercive fields together with the particular effects at certain magnetic fields shown in the hysteresis loops induce to believe that a growing amount of Nd induces stronger and stronger magnetocrystalline anisotropies due to the spin–orbit coupling, absent in Gd, which, in its turn, would induce a stronger narrow-domain-wall pinning,[21] as it happens in many other materials.[21,24–26]

This description of the magnetic properties is further supported by the study of the magnetization isotherms, which present different behavior depending on the temperature range, applied field, and composition of the sample. $Nd_{0.15}Gd_{2.85}CoNi$ presents a ferromagnetic behavior in the full temperature and field range, as proved by the magnetization being smaller from one isotherm to the next one at a higher temperature (see Fig. S2 in the supplementary material). The other three, while they do have this behavior at temperatures higher than about 50 K, they present a different one at lower temperatures.

Figure S2 in the supplementary material shows the whole set of field dependent magnetization curves while Fig. 6 show the details that are relevant. Starting with $Nd_{0.5}Gd_{2.5}CoNi$, below about 1.5 T and 50 K, the behavior is antiferromagnetic (every isotherm presents a higher magnetization than the previous one). At higher fields, most isotherms (save for those at the lowest temperatures) turn to a ferromagnetic behavior, but even at the highest field applied, at temperatures lower than 14 K, antiferromagnetic features prevail. In $NdGd_2CoNi$, the behavior is even more complex. At low temperatures, low field, the behavior of the isotherms is antiferromagnetic. As field increases there is a tendency for the isotherms to gather closely, to spread again and arrive to a fully ferromagnetic behavior for fields higher than 2 T. Finally, for $Nd_{1.5}Gd_{1.5}CoNi$, there is antiferromagnetic behavior at very low fields that very quickly turns into a common ferromagnetic behavior.

Adding up all this information, it can be sustained that at low temperature (in some cases at a low field, in other cases even at high field), the magnetic arrangement is extremely complex, with some AFM features. Neutron diffraction studies would be needed in order to clarify these states.

C. Critical behavior

In this section, the study of the critical behavior of the PM-FM transition is performed. Critical behavior theory assesses that several

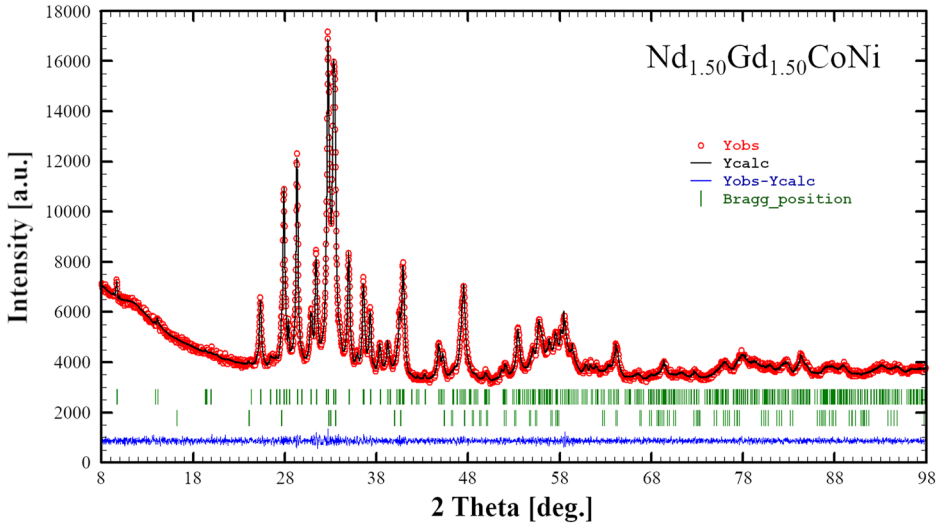

FIG. 2. Observed x-ray powder pattern (red circle), and Rietveld refinement profile (black line) for the sample $Nd_{1.50}Gd_{1.50}CoNi$. The lower profile (blue line) gives the difference between observed and calculated data; the Bragg angle positions are indicated by vertical bars (green). The upper row of Bragg positions is the $Nd_{1.51(3)}Gd_{1.49(3)}CoNi$ compound (Dy_3Ni_2-type, *mS*20, *C*2/*m*, No. 12) (final refined composition), the lower row is $Nd_{0.40}Gd_{0.60}Co_{0.40}Ni_{0.60}$ (CrB-type, *oS*8, *Cmcm*, No. 63) (composition as from SEM-EDX).

physical variables present a critical behavior in the near vicinity of the critical temperature of second order phase transitions, fulfilling the following equations as a function of the reduced temperature $t = (T - T_C)/T_C$,[27] such as the spontaneous magnetization $M_S(T)$,

$$M_S(T) \sim |t|^{\beta} \quad (T < T_C), \tag{1}$$

the inverse of the initial susceptibility

$$\chi_0^{-1}(T) \sim |t|^{\gamma} \quad (T > T_C), \tag{2}$$

and the magnetization at the critical temperature

$$M(H) \sim H^{1/\delta} \quad (T = T_C), \tag{3}$$

while the magnetic equation of state

$$M(H,t) = |t|^{\beta} f_{\pm}\left(H/|t|^{\beta+\gamma}\right), \tag{4}$$

must be fulfilled in the critical region.

A customary procedure has been followed to obtain the critical exponents (β, γ, and δ).[28,29] To start with, the standard Arrott Plot (M^2 isotherms as a function of H/M in the near vicinity of T_C) has been drawn, as well as the Modified Arrott Plots (MAP), plotting $M^{1/\beta}$ vs $(H/M)^{1/\gamma}$ for the Heisenberg [$\beta = 0.3689(3)$, $\gamma = 1.3960(9)$][30] and Ising universality classes [$\beta = 0.326\,53(10)$, $\gamma = 1.2373(2)$].[31] The standard Arrott Plot corresponds to the case of the mean field universality class ($\beta = 0.5$, $\gamma = 1$). This is also related to the Banerjee criterion, which states that if all isotherms in this plot have positive slopes, the transition is second order,[32] what happens in all cases (see

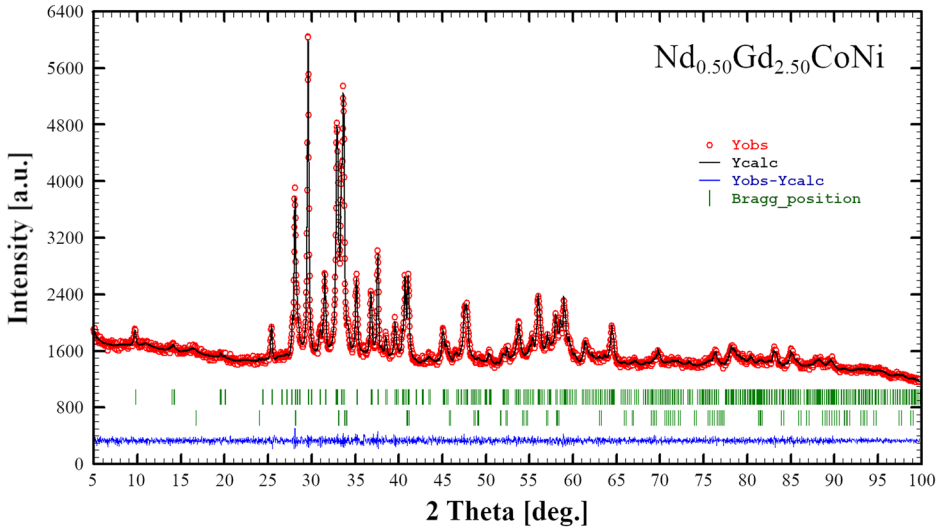

FIG. 3. Observed x-ray powder pattern (red circle), and Rietveld refinement profile (black line) for the sample $Nd_{0.50}Gd_{2.50}CoNi$. The lower profile (blue line) gives the difference between observed and calculated data; the Bragg angle positions are indicated by vertical bars (green). The upper row of Bragg positions is the $Nd_{0.48(6)}Gd_{2.52(6)}CoNi$ compound (Dy_3Ni_2-type, *mS*20, *C*2/*m*, No. 12 (final refined composition) the lower row is $Nd_{0.13}Gd_{0.87}Co_{0.40}Ni_{0.60}$ (CrB-type, *oS*8, *Cmcm*, No. 63) (composition as from SEM-EDX).

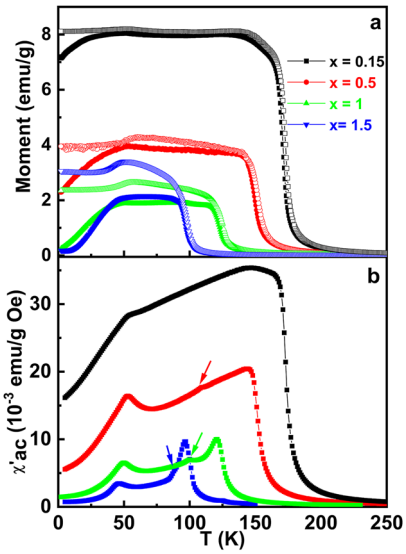

FIG. 4. (a) Magnetization as a function of temperature in zero-field cooled (filled-in symbols) and field-cooled (empty symbols) mode with applied field $\mu_0 H = 100$ Oe. (b) Real part of the *ac* susceptibility at $f = 100$ Hz. The arrows denote the structure explained in the text.

Fig. S3 in the supplementary material), confirming the character of the transition and justifying this critical behavior study.

Starting with the plot that gives a better ensemble of straight and parallel lines, an iterative process is performed until it converges. This consists of taking a linear extrapolation of these isotherms from the high field values to extract $(M_S)^{1/\beta}$ and $(\chi_0^{-1})^{1/\gamma}$ as an intercept on $M^{1/\beta}$ and $(H/M)^{1/\gamma}$ axis, respectively. These values of $M_S(T)$ and $\chi_0^{-1}(T)$ have been independently fitted to Eqs. (1) and (2), extracting new values of β and γ. With these values new MAPs are drawn, new extrapolations are done, and so forth until the values of the critical exponents converge and the best parallelism is obtained in the MAPs. Figure 7 shows the final modified Arrott plot and the fittings for $Nd_{1.5}Gd_{1.5}CoNi$, while the rest can be found in Fig. S4 in the supplementary material. Table III displays the obtained critical exponents.

Second, the Kouvel-Fisher method has been used: from a linear fitting of $M_S(dM_S/dT)^{-1}$ and $\chi_0^{-1}(d\chi_0^{-1}/dT)^{-1}$ with respect to temperature, β and γ are obtained as the inverse of the slopes. Figure 8 shows the fittings for $Nd_{0.15}Gd_{2.85}CoNi$ and $Nd_{1.5}Gd_{1.5}CoNi$, the other two are in Fig. S5 in the supplementary material. Table III contains the exponents thus obtained, which are in good agreement to the ones obtained with the MAPs.

The next step consists of plotting the critical isotherms to extract the critical exponent δ by fitting the experimental curve

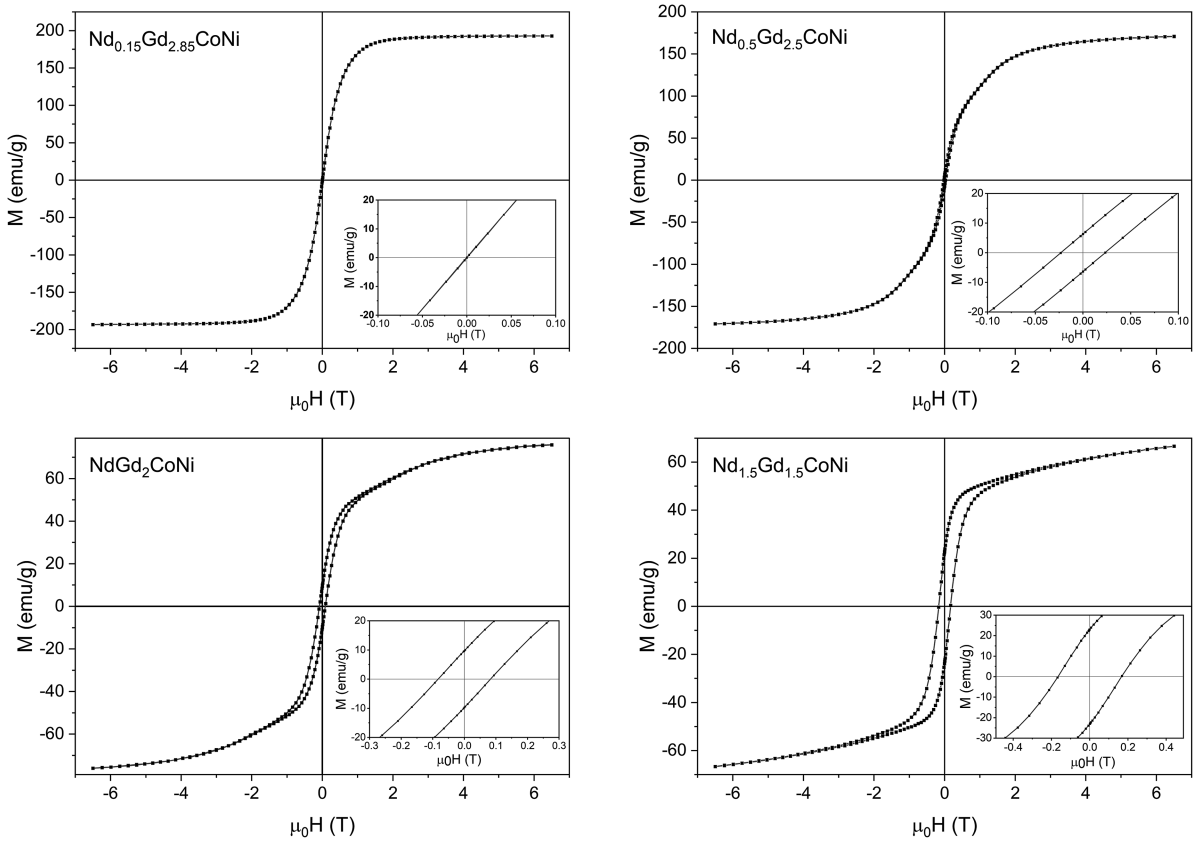

FIG. 5. Hysteresis loops at 2 K for the four magnetic samples. The insets show the coercive fields.

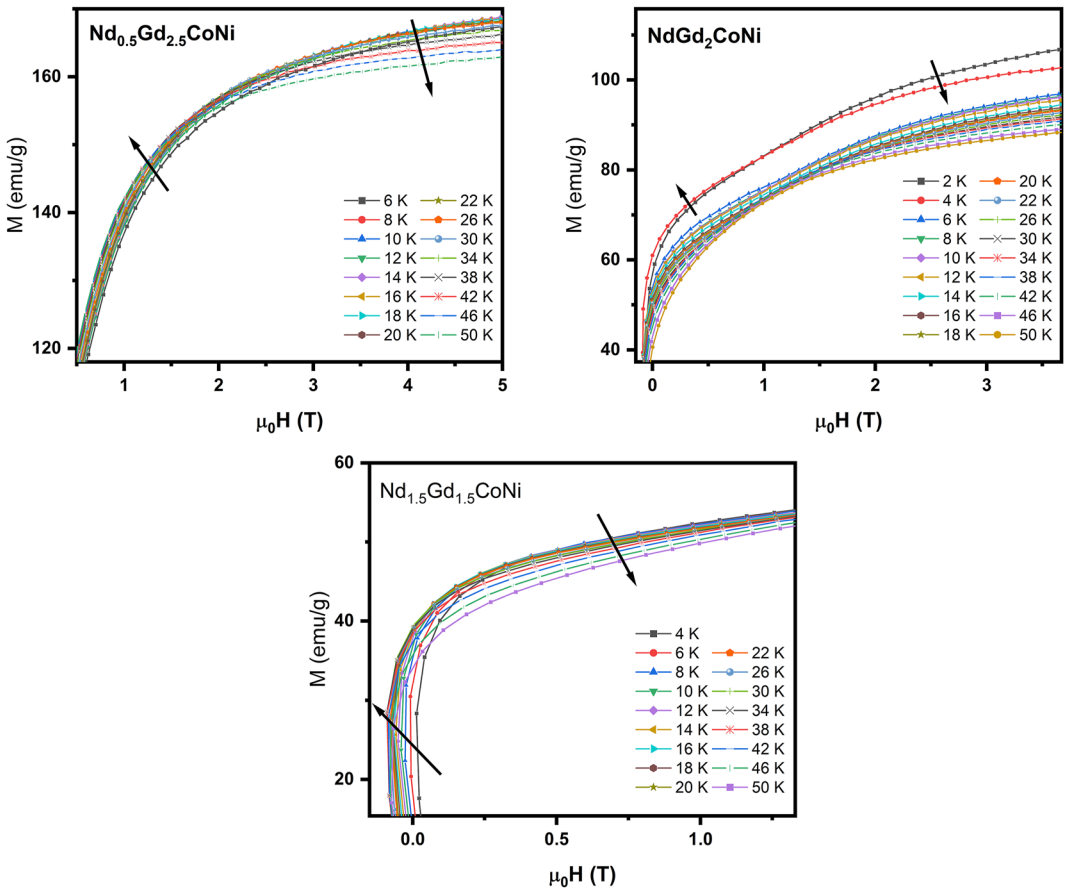

FIG. 6. Details of the magnetization isotherms at low temperatures for $Nd_{0.5}Gd_{2.5}CoNi$, $NdGd_2CoNi$ and $Nd_{1.5}Gd_{1.5}CoNi$.

to Eq. (3). Figure 9 shows them in a log-log scale, for two compounds (the other two can be found in Fig. S6 in the supplementary material). The value thus obtained can be compared with the one calculated using the Widom scaling equation:[27]

$$\delta = 1 + \gamma/\beta, \tag{5}$$

with a good agreement, as shown in Table III.

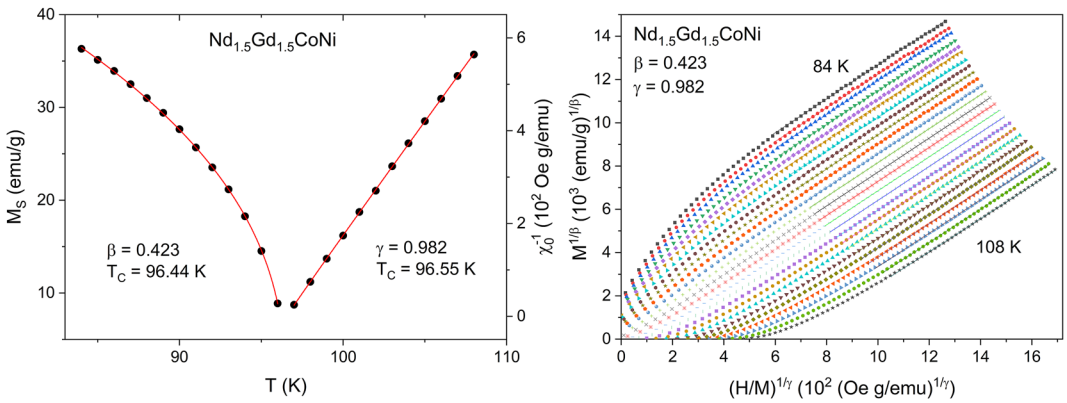

FIG. 7. Left column: Spontaneous magnetization (left) and inverse of initial susceptibility (right) vs temperature for $Nd_{1.5}Gd_{1.5}CoNi$. The solid curves correspond to the fits to Eqs. (1) and (2), as explained in the text. Right column: optimized Modified Arrot Plot.

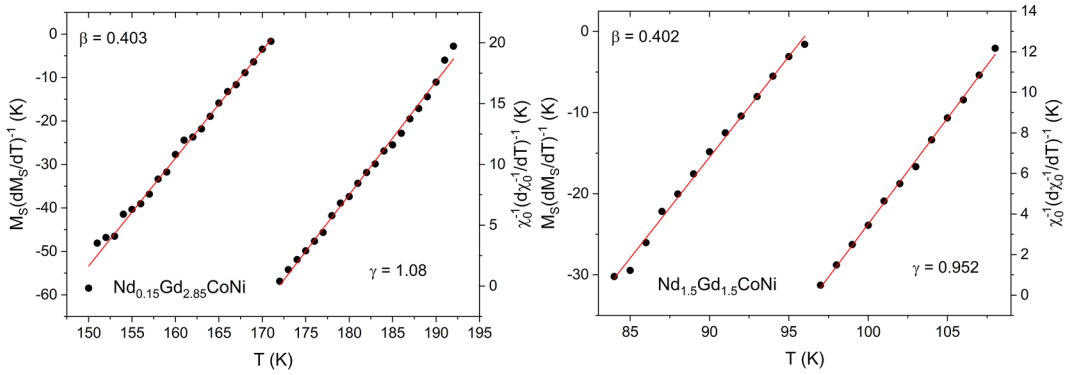

FIG. 8. Kouvel-Fisher plot of spontaneous magnetization (left) and inverse of initial susceptibility (right) for $Nd_{0.15}Gd_{2.85}CoNi$ and $Nd_{1.5}Gd_{1.5}CoNi$. The straight lines are linear fits, from that the critical exponents are obtained.

The last step to confirm the validity of the critical exponents obtained so far is to check if they fulfill the magnetic equation of state Eq. (4). If this is so, the magnetization isotherms must collapse onto two independent branches, one for those above T_C, another one for those below it. Figure 10 shows a very good agreement with theory for $Nd_{0.5}Gd_{2.5}CoNi$ and $NdGd_2CoNi$ ($Nd_{0.15}Gd_{2.85}CoNi$ and $Nd_{1.5}Gd_{1.5}CoNi$ can be found in Fig. S7 in the supplementary material).

For each compound, the values derived from the different methods agree reasonably well. These results indicate that none of them belongs to a well-defined universality class. The values lie between the mean-field and 3D Heisenberg universality classes, with no defined evolution with increasing Nd content. Three compositions (x = 0.15, 0.5, and 1.5) basically share common values of β (around 0.4) and γ (around 1) while the intermediate compound with x = 1 has $\beta = 0.46$ and $\gamma = 1.22$. In the first case, $\beta = 0.4$ is closer to the 3D-Heisenberg case ($\beta_{Heis} = 0.369$) than to the mean-field one ($\beta_{MF} = 0.5$) while $\gamma = 1$ agrees with the mean-field ($\gamma_{MF} = 1$, $\gamma_{Heis} = 1.396$). Renormalization group analysis assesses that the range of the exchange interaction $J(r)$ is determined by the critical parameter γ ($\gamma = 1$ corresponds to long-range ordering),[33] which would mean that long-range order interactions are responsible for this transition in $Nd_{0.15}Gd_{2.85}CoNi$, $Nd_{0.5}Gd_{2.5}CoNi$, and $Nd_{1.5}Gd_{1.5}CoNi$ but with a marked deviation from the mean-field model, as far as the β exponent goes. On the other hand, for the particular composition $NdGd_2CoNi$, the value of γ agrees with the Ising model (short-range interactions, uniaxial anisotropy), while β is closer to the mean-field model.

The critical behavior of the PM-FM transition in pure Gd has been studied by several groups using different techniques and it is far from clear. The values of β have been found to be, in general, close to the 3D-Heisenberg universality class (but higher in some cases) while those for γ are close to the 3D-Ising one.[34] In other intermetallic materials that contain Gd, the studies on critical behavior have also pointed to a 3D Heisenberg universality class with small deviations,[35,36] taking into account that the magnetic properties solely arise from the rare-earth atom and not from the transition metals. On the other hand, it has been suggested in Gd_3CoNi that

TABLE III. Critical exponents.

Material	Technique	β	γ	δ
$Nd_{0.15}Gd_{2.85}CoNi$	Modified Arrott plot	0.403 ± 0.003	1.08 ± 0.01	3.68[a] ± 0.03
	Kouvel-Fisher method	0.403 ± 0.008	1.08 ± 0.01	3.68[a] ± 0.06
	Critical isotherm			3.93 ± 0.01
$Nd_{0.5}Gd_{2.5}CoNi$	Modified Arrott plot	0.409 ± 0.002	1.04 ± 0.01	3.54[a] ± 0.03
	Kouvel-Fisher method	0.38 ± 0.01	1.08 ± 0.02	3.84[a] ± 0.1
	Critical isotherm			3.757 ± 0.006
$NdGd_2CoNi$	Modified Arrott plot	0.47 ± 0.005	1.22 ± 0.03	3.60[a] ± 0.07
	Kouvel-Fisher method	0.45 ± 0.01	1.22 ± 0.02	3.71[a] ± 0.07
	Critical isotherm			3.671 ± 0.008
$Nd_{1.5}Gd_{1.5}CoNi$	Modified Arrott plot	0.423 ± 0.003	0.982 ± 0.007	3.32[a] ± 0.02
	Kouvel-Fisher method	0.402 ± 0.008	0.952 ± 0.009	3.37[a] ± 0.05
	Critical isotherm			3.282 ± 0.002

[a]Calculated from Eq. (5) $\delta = 1 + \gamma/\beta$.

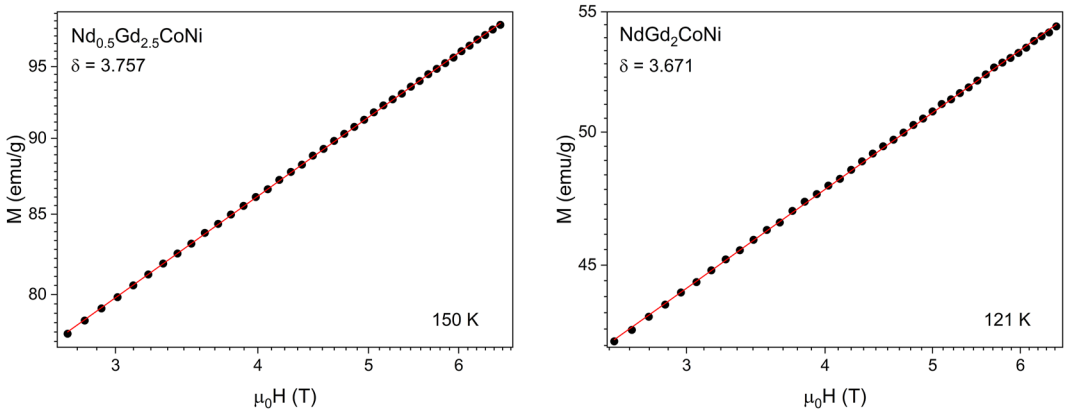

FIG. 9. M vs $\mu_0 H$ plot in a log-log scale collected at critical isotherms for $Nd_{0.5}Gd_{2.5}CoNi$ and $NdGd_2CoNi$. The straight line, in each case, is the linear fit from that the exponent δ is obtained.

the magnetic interactions are long-range order,[11] with which the values of γ here found agree. In what concerns the values of β, there is now a deviation from the Heisenberg model, surely due to the presence of Nd, which introduces magnetocrystalline anisotropies. The role of Co and Ni cannot be completely ruled out, either. Though in Tb_3CoNi, neither Co nor Ni present a magnetic moment,[12] a small one has been found for Co in Gd_3CoNi.[11]

Therefore, neutron diffraction measurements should be needed to ascertain the complexity of the spin arrangement for this PM-FM transition, as well.

D. Magnetocaloric properties

The magnetic entropy change has been indirectly evaluated using the well-known Maxwell relation:

$$\Delta S_M(T, \Delta' H) = \mu_0 \int_{H_i}^{H_f} \left(\frac{\partial M}{\partial T}\right)_H dH. \tag{6}$$

The results are shown in Fig. 11 where it is seen that there is a relevant direct magnetocaloric effect for all of them, centered at T_C. The values for $Nd_{0.15}Gd_{2.85}CoNi$ are equivalent to the ones published for Gd_3CoNi.[11] The effect of Nd is to reduce the maximum, while tuning it to other temperatures (those for the different T_C). The spin reorientation transition, which takes place at around 50 K gives an asymmetric shape to the peak. Table IV presents the maximum values of the curves $\left|\Delta S_M^{pk}\right|$ for $\mu_0 \Delta H$ = 2, 5 and 6.9 T, together with the refrigerant capacities:

$$RC_{FWHM} = \left|\Delta S_M^{pk}\right| \delta T_{FWHM}, \tag{7}$$

where δT_{FWHM} is the temperature width of the magnetic entropy change at half maximum (FWHM) and

$$RC_{Area} = \int_{T_{cold}}^{T_{hot}} \Delta S_M(T, \Delta H) dT, \tag{8}$$

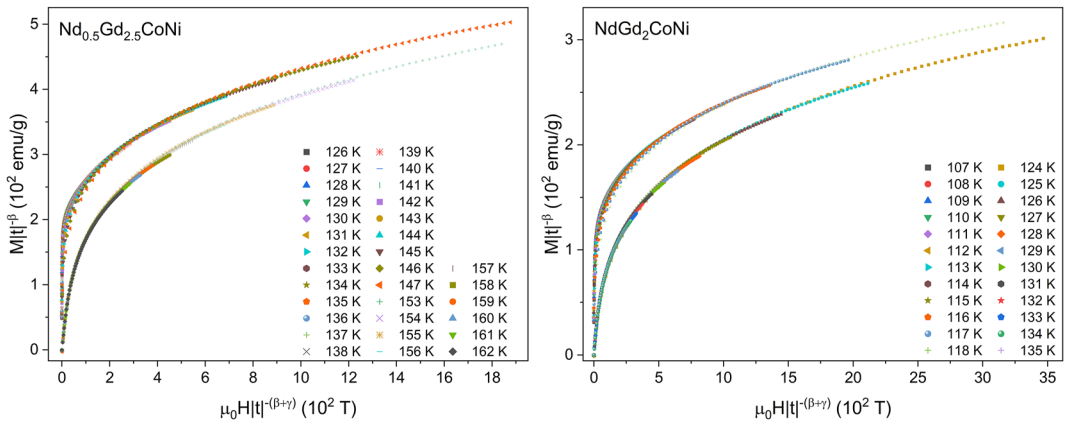

FIG. 10. The renormalized magnetization plotted as a function of the renormalized field following Eq. (4) for $Nd_{0.5}Gd_{2.5}CoNi$ and $NdGd_2CoNi$.

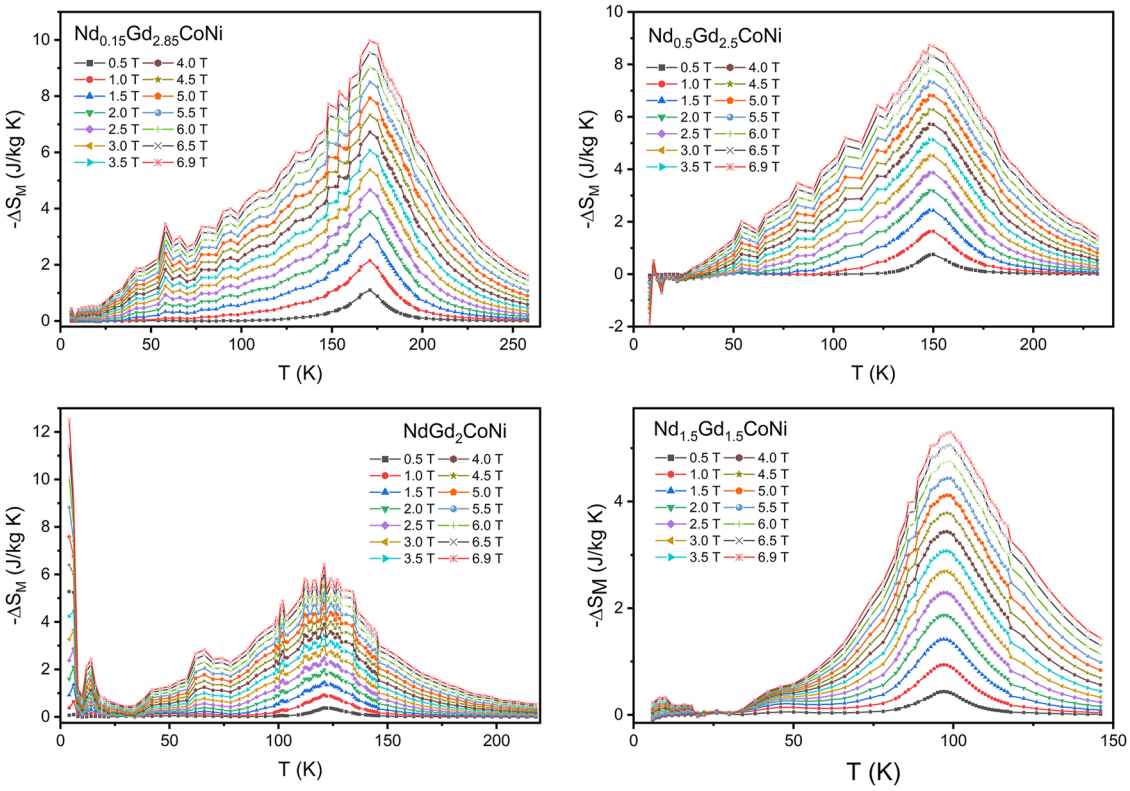

FIG. 11. Magnetic entropy change $-\Delta S_M$ for $\mu_0 \Delta H$ from 0.5 T to 6.9.

which is the area enclosed by the magnetic entropy change vs temperature curve in the range enclosed by the full width at half maximum. It is important to compare the values of the magnetic entropy change and the refrigerant capacities with other rare-earth based materials in their respective temperature ranges, including other Gd-based intermetallic compounds and, as it turns out, they are quite competitive though they are not among the highest ones.[2,5,8,11] We will also see in Sec. III E that the thermal diffusivity is

TABLE IV. Maximum of the magnetic entropy change $\left|\Delta S_M^{pk}\right|$ and refrigerant capacities RC_{FWHM}, RC_{Area} at applied fields $\mu_0 \Delta H$ (2, 5 and 6.9 T) for the direct magnetocaloric effect at T_C. The indicated temperatures correspond to the position of the maximum of $-\Delta S_M$.

		$Nd_{0.15}Gd_{2.85}CoNi$ T_C = 171 K	$Nd_{0.5}Gd_{2.5}CoNi$ T_C = 148 K	$NdGd_2CoNi$ T_C = 121 K	$Nd_{1.5}Gd_{1.5}CoNi$ T_C = 98 K
2 T	$\left\|\Delta S_M^{pk}\right\|$ (J kg^{-1} K^{-1})	3.9	3.2	2.0	1.9
	RC_{FWHM} (J kg^{-1})	189	152	74	52
	RC_{Area} (J kg^{-1})	140	113	55	41
5 T	$\left\|\Delta S_M^{pk}\right\|$ (J kg^{-1} K^{-1})	7.9	6.8	4.8	4.1
	RC_{FWHM} (J kg^{-1})	663	536	255	166
	RC_{Area} (J kg^{-1})	458	399	187	129
6.9 T	$\left\|\Delta S_M^{pk}\right\|$ (J kg^{-1} K^{-1})	10.0	8.7	6.4	5.3
	RC_{FWHM} (J kg^{-1})	896	763	367	248
	RC_{Area} (J kg^{-1})	657	577	268	192

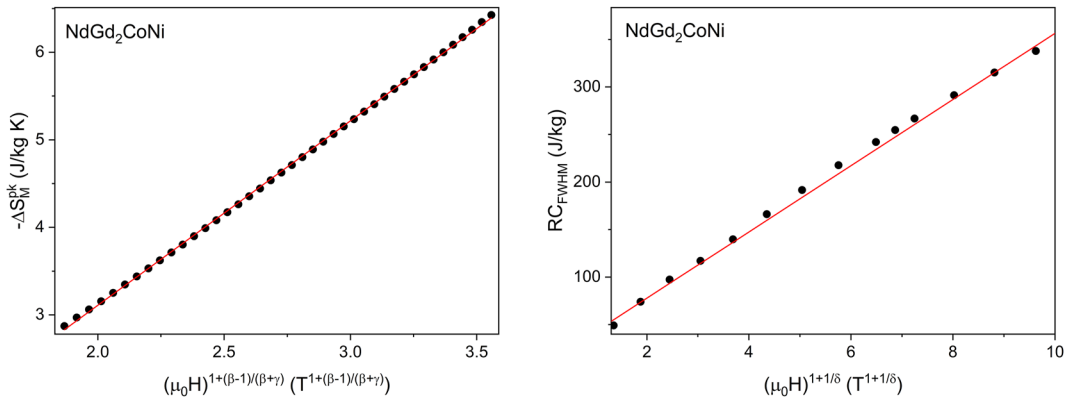

FIG. 12. Field dependence of the peak magnetic entropy change and the refrigerant capacity RC_{FWHM} for $NdGd_2CoNi$.

high enough so that these materials can be considered as promising magnetocaloric materials in real applications.

At low temperature we can find additional and specific magnetocaloric effects, depending on the amount of Nd, which is related to the magnetic properties already studied in Sec. III B. $Nd_{0.5}Gd_{2.5}CoNi$ presents a small inverse magnetocaloric effect due to the antiferromagnetic behavior observed in that region (see Fig. 6). This effect has also been found in some other members of the family R_3CoNi (R = Tb, Dy, and Er).[13] $Nd_{1.5}Gd_{1.5}CoNi$ also shows a small inverse magnetocaloric effect that quickly turns to a direct one, as the field is applied, which agrees with the acquisition of full ferromagnetic properties at a low field. However, these phenomena are small

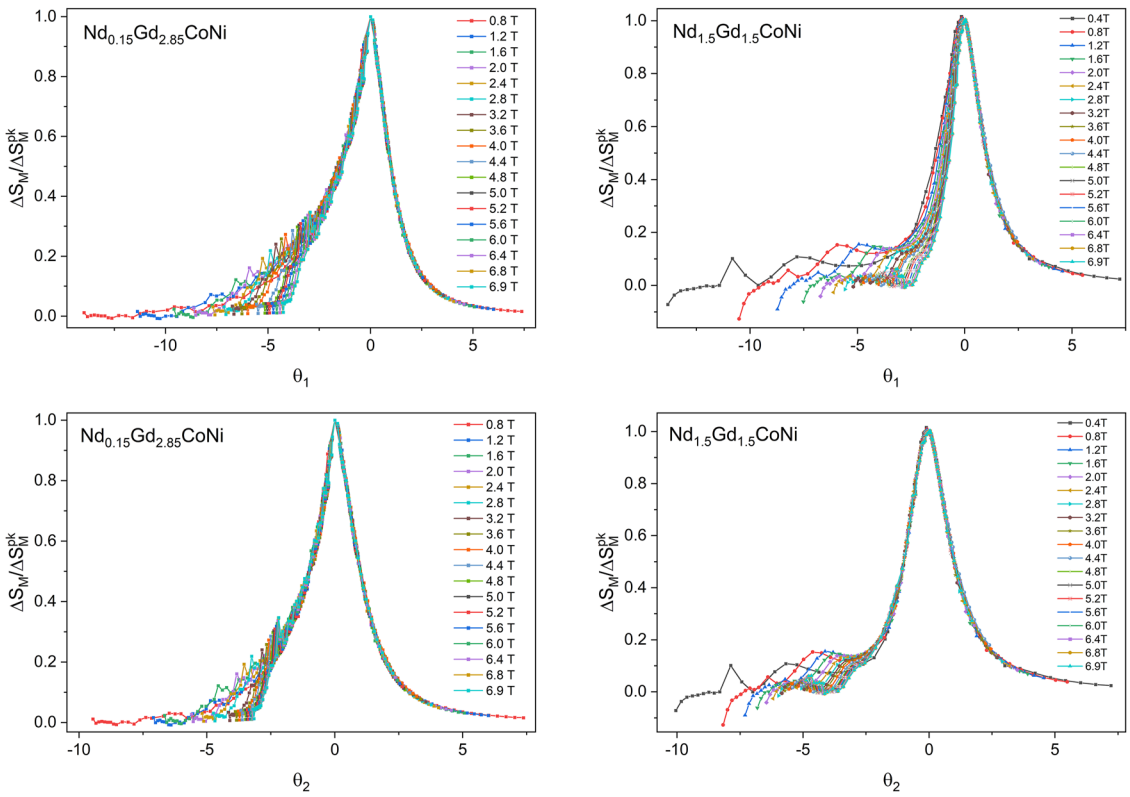

FIG. 13. Universal curve with the rescaled magnetic entropy changes using one (above) and two (below) reference temperatures, for $Nd_{0.15}Gd_{2.85}CoNi$ and $Nd_{1.5}Gd_{1.5}CoNi$.

and have no practical applications. What is extremely interesting is the important direct magnetocaloric effect at very low temperature for $NdGd_2CoNi$, which could be useful for cryogenic applications and whose origin lies in the magnetic properties above explained.

The critical behavior study performed in Sec. III C can now be completed taking into account that the magnetic entropy change scales in the following way:[37,38]

$$\Delta S_M^{pk} \sim H^{1+(1/\delta)(1-1/\beta)}, \tag{9}$$

whereas the refrigerant capacity scales as[37,38]

$$RC \sim H^{1+1/\delta}. \tag{10}$$

Figure 12 presents these scalings for the case of $NdGd_2CoNi$, the rest being shown in Fig. S8 in the supplementary material, using the values of β and δ obtained in Sec. III B. This confirms the validity of the critical exponents contained in Table III.

To end this analysis, universal curves have been built for the magnetic entropy change. As the PM-FM transitions have been found to be second order, it is possible to normalize the curves and show that they superimpose in the close vicinity of the critical temperature, using the procedure proposed by Franco *et al.*[37,39] To this end, the magnetic entropy change is normalized with its peak value and the temperature axis is rescaled, using either one or two reference temperatures. In the latter case, the scaling of the temperature axis, in this case, is as follows:

$$\theta_2 = \begin{cases} -(T - T_C)/(T_{r1} - T_C), & T \le T_C, \\ (T - T_C)/(T_{r2} - T_C), & T > T_C. \end{cases} \tag{11}$$

Figure 13 shows the result for $Nd_{0.15}Gd_{2.85}CoNi$ and $Nd_{1.5}Gd_{1.5}CoNi$ (the rest can be found in Fig. S9 in the supplementary material), where the overlapping in the critical region is not good for only one reference temperature but perfect with two, confirming the second order nature of the PM-FM transition.

In the low temperature region, far from the critical region (where the critical theory is not fulfilled), there is no superposition. Nevertheless, it is common that, if there is no other phase transition, the superposition be good in the full temperature range. In this particular case, we do have other magnetic effects at low temperature, which affect these curves. It has already been shown that whenever there are spin reorientation phenomena below the main peak, distortions from scaling appear.[40]

Concerning the differences in the critical region between using one and two reference temperatures (see it especially for $Nd_{1.5}Gd_{1.5}CoNi$), it has been theorized that the deviations close to the critical region can be due to demagnetization effects or to the presence of another magnetic phase with a much higher T_C than the one of the transition under study. In the former case, the

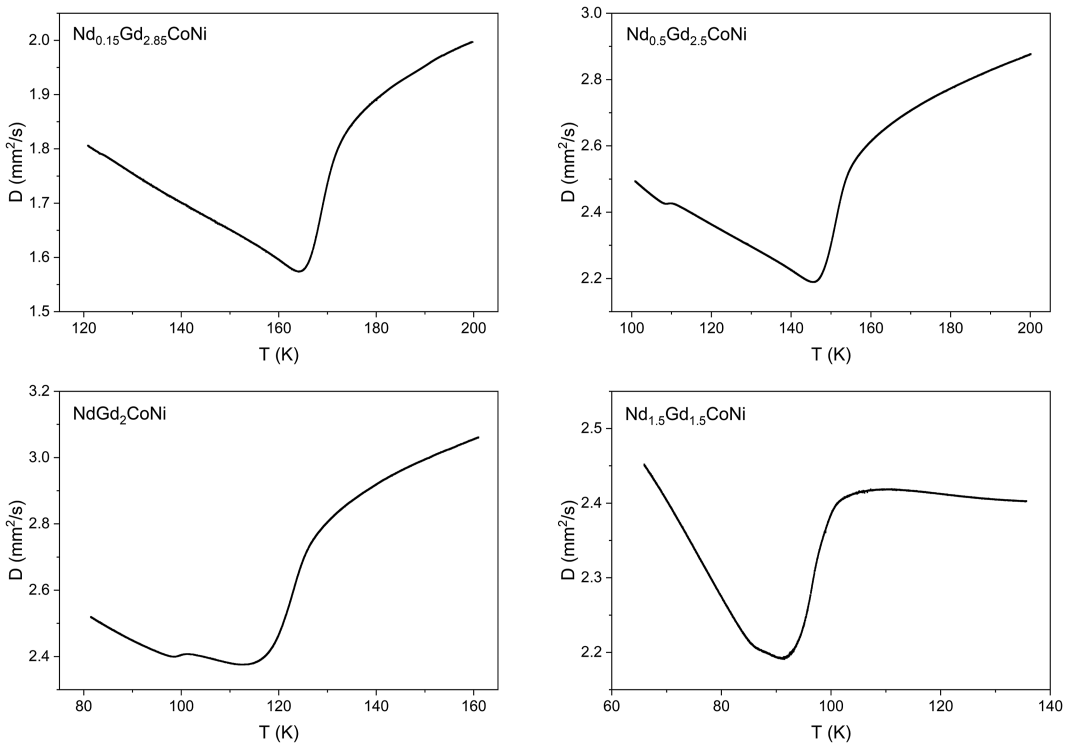

FIG. 14. Thermal diffusivity as a function of temperature for the four compounds.

curves below T_C would move to higher values as the magnetic field increases, while in the latter the effect would be the opposite.[41,42] This last effect is the one that takes place here but there is no hint of any other magnetic transition above T_C in any measurement. In addition, it has been found that, in other single-phase Gd-alloys, the lower the critical temperature, the stronger this effect,[38] while it has also been observed in other rare-earths compounds.[13,43,44] It is worth noting the interest of these universal curves, as they allow the extrapolation of the whole magnetic entropy change curve to non-accessible magnetic fields.

E. Thermal properties

An aspect seldom studied in many magnetocaloric materials is their thermal transport properties; they must be good enough so that the material can undergo the magnetic cycles in a practical appliance and conduct and exchange heat fast enough to work at high frequencies.[1,45] Thermal diffusivity D is the variable that reflects how quick heat is transferred in any material in a non-steady situation, following the equation:[46]

$$\nabla^2 T(\vec{\boldsymbol{r}}, t) + \frac{g(\vec{\boldsymbol{r}}, t)}{K} = \frac{1}{D}\frac{\partial T(\boldsymbol{r}, t)}{\partial t}, \tag{12}$$

where $T(\boldsymbol{r}, t)$ is the temperature field as a function of the position vector and time, $g(\boldsymbol{r}, t)$ is the heat generated in the medium per unit time and unit volume, K is the thermal conductivity. K and D are related by the following equation:

$$D = \frac{K}{\rho c_p}, \tag{13}$$

where ρ is the density and c_p the specific heat.

Figure 14 shows the thermal diffusivity as a function of temperature around the PM-FM transition, where this is signaled by the sudden reduction of D as temperature decreases. The values of D are in the range 1.5–3 mm^2/s, which are comparable to the values exhibited by good magnetocaloric materials such as $Gd_5Si_2Ge_2$, $La(Fe_{0.88}Si_{0.12})_{13}$, and one order of magnitude higher than MnAs.[45] Detailed heating and cooling runs at very small temperature rates have shown that there is no thermal hysteresis in this transition, confirming the second order character, which is extremely relevant to efficiently work in a cycle. It is worth noting that, at a lower temperature, there are additional small steps in $Nd_{0.5}Gd_{2.5}CoNi$ and $NdGd_2CoNi$ that correspond to the small peaks also obtained in the *ac* magnetic susceptibility shown in Fig. 4(b).

IV. CONCLUSIONS

A full study of the $Nd_xGd_{3-x}CoNi$ series (x = 0.15, 0.5, 1, and 1.5) has been undertaken, covering the crystal structure, the magnetic, and magnetocaloric properties, as well as the critical behavior of the PM-FM second order phase transitions. All these phases crystallize with the monoclinic Dy_3Ni_2-type (*mS*20, *C*2/*m*, No. 12), as the parent compound Gd_3CoNi does. Nd doping leads to an isotropic increase of the three lattice parameters *a*, *b*, *c*, and to a decrease of parameter β, with the result of an increase in the unit-cell volume, as expected due to Nd having a larger atomic volume than Gd.

The magnetic study has revealed that all compounds present a paramagnetic to ferromagnetic (PM-FM) second order phase transition with decreasing Curie temperature as the Nd concentration is increased (T_C = 171, 150, 120, and 96 K, for x = 0.15, 0.5, 1, and 1.5 respectively). The introduction of Nd alters the magnetic ground state, inducing a reorientation of the ferromagnetic spins at lower temperature (<50 K), as revealed by the *ac* susceptibility measurements and the magnetization isotherms at low temperature. The shape of the hysteresis loops at 2 K, together with the appearance of a growing coercive field as Nd doping is increased, indicate that Nd introduces magnetocrystalline anisotropies due to the spin–orbit coupling, which would be responsible for a narrow-domain-wall pinning and, therefore, the observed thermomagnetic irreversibility.

The critical exponents (β, γ, and δ) for the PM-FM transitions have been found. On the one hand, in x = 0.15, 0.5, and 1.5 the value of $\gamma \approx 1$ indicates that the magnetic interactions are long-range order while the values of β point to a certain deviation from the 3D-Heisenberg universality class (as is common in Gd-based intermetallic materials); on the other hand, $NdGd_2CoNi$ has a particular critical behavior, as manifested by a β value close to the mean field model while γ is close to the uniaxial 3D-Ising one. As for the MCE, this can be tuned with Nd doping to a particular region of interest, maintaining competitive values in the magnetic entropy change and the refrigerant capacity, compared with other rare-earth based intermetallic materials. A very interesting point is the comparatively large MCE observed in $NdGd_2CoNi$ at very low temperature, with possible cryogenic applications. The universal curves for the MCE as well as the scaling of magnetic entropy change and the refrigerant capacity, confirm the critical behavior study done with the magnetic measurements. The study of the thermal properties of the compounds to ensure that they could be working in real refrigeration appliances in quick cycles has given that the thermal diffusivity is extremely competitive, as it is in the range 1.5–3 mm^2/s.

SUPPLEMENTARY MATERIALS

See the supplementrary materials for the supplementary figures mentioned in the text.

ACKNOWLEDGMENTS

This work has been supported by Departamento de Educación del Gobierno Vasco (Project No. IT1430-22). The authors thank for technical and human support provided by SGIker of UPV/EHU.

AUTHOR DECLARATIONS

Conflict of Interest

The authors have no conflicts to disclose.

Author Contributions

A. Oleaga: Conceptualization (lead); Funding acquisition (lead); Investigation (lead); Methodology (lead); Supervision (lead); Writing – original draft (lead); Writing – review & editing (lead).

A. Erkoreka: Data curation (equal); Formal analysis (equal); Investigation (equal); Software (equal); Writing – review & editing (supporting). **A. Herrero**: Formal analysis (equal); Investigation (equal); Validation (equal); Writing – review & editing (supporting). **A. Provino**: Data curation (equal); Investigation (equal); Validation (equal); Writing – original draft (equal); Writing – review & editing (equal). **D. Peddis**: Formal analysis (equal); Investigation (equal); Writing – original draft (equal); Writing – review & editing (equal). **P. Manfrinetti**: Conceptualization (equal); Data curation (equal); Formal analysis (equal); Methodology (equal); Writing – original draft (equal); Writing – review & editing (equal).

DATA AVAILABILITY

The data that support the findings of this study are available from the corresponding author upon reasonable request.

REFERENCES

[1]T. Gotschall, K. P. Skokov, M. Fries, A. Taubel, I. Radulov, F. Scheibel, D. Benke, S. Riegg, and O. Gutfleisch, "Making a cool choice: The materials library of magnetic refrigeration," Adv. Energy Mater. **9**, 1901322 (2019).

[2]V. Franco, J. S. Blázquez, J. J. Ipus, J. Y. Law, L. M. Moreno-Ramírez, and A. Conde, "Magnetocaloric effect: From materials research to refrigeration devices," Prog. Mater. Sci. **93**, 112–232 (2018).

[3]A. M. Tishin, "A review and new perspectives of the magnetocaloric effect: New materials and local heating and cooling inside the human body," Int. J. Refrig. **68**, 177–186 (2016).

[4]K. A. Gschneidner, Jr., V. K. Pecharsky, and A. O. Tsokol, "Recent developments in magnetocaloric materials," Rep. Prog. Phys. **68**, 1479–1539 (2005).

[5]L.-W. Li, "Review of magnetic properties and magnetocaloric effect in the intermetallic compounds of rare earth with low boiling point," Chin. Phys. B **25**, 037502 (2016).

[6]V. Franco, J. S. Blázquez, B. Ingale, and A. Conde, "The magnetocaloric effect and magnetic refrigeration near room temperature: Materials and models," Annu. Rev. Mater. Res. **42**, 305–342 (2012).

[7]H. Zhang, R. Gimaev, B. Kovalev, K. Kamilov, and V. Zverev, "Review on the materials and devices for magnetic refrigeration in the temperature range of nitrogen and hydrogen liquefaction," Phys. B **558**, 65–73 (2019).

[8]Y. Zhang, "Review of the structural, magnetic and magnetocaloric properties in ternary rare earth RE_2T_2X type intermetallic compounds," J. Alloys Compd. **787**, 1173–1186 (2019).

[9]J. Y. Law and V. Franco, "Magnetocaloric composite materials," *Encyclopedia of Materials: Composites* (Elsevier, 2021).

[10]J. Y. Law and V. Franco, "Pushing the limits of magnetocaloric high-entropy alloys," APL Mater. **9**, 080702 (2021).

[11]A. Provino, V. Smetana, D. Paudyal, K. A. Gschneidner, Jr., A.-V. Mudring, V. K. Pecharsky, P. Manfrinetti, and M. Putti, "Gd_3Ni_2 and $Gd_3Co_xNi_{2-x}$: Magnetism and unexpected Co/Ni crystallographic ordering," J. Mater. Chem. C **4**, 6078–6089 (2016).

[12]C. Ritter, A. Provino, F. Fauth, S. K. Dhar, V. K. Pecharsky, and P. Manfrinetti, "From Tb_3Ni_2 to Tb_3CoNi: The interplay between chemistry, structure, and magnetism," Phys. Rev. Mater. **3**, 024406 (2019).

[13]A. Herrero, A. Oleaga, A. Provino, I. R. Aseguinolaza, A. Salazar, D. Peddis, and P. Manfrinetti, "Crystallographic, magnetic and magnetocaloric properties in novel intermetallic materials R_3CoNi (R = Tb, Dy, Ho, Er, Tm, Lu)," J.Alloys Compd. **865**, 158948 (2021).

[14]K. Yvon, W. Jeitschko, and E. Parthé, "*LAZY PULVERIX*, a computer program, for calculating X-ray and neutron diffraction powder patterns," J. Appl. Crystallogr. **10**, 73–74 (1977).

[15]J. Rodríguez-Carvajal, "Recent advances in magnetic structure determination by neutron powder diffraction," Physica B **192**, 55–69 (1993).

[16]H. Neves Bez, H. Yibole, A. Pathak, Y. Mudryk, and V. K. Pecharsky, "Best practices in evaluation of the magnetocaloric effect from bulk magnetization measurements," J. Magn. Magn. Mater. **458**, 301–309 (2018).

[17]W. Jiang, X. Z. Zhou, G. Williams, Y. Mukovskii, and K. Glazyrin, "Critical behavior and transport properties of single crystal $Pr_{1-x}Ca_xMnO_3$ (x = 0.27, and 0.29)," Phys. Rev. B **78**, 144409 (2008).

[18]W. Jiang, X. Z. Zhou, G. Williams, Y. Mukovskii, and K. Glazyrin, "Griffiths phase and critical behavior in single-crystal $La_{0.7}Ba_{0.3}MnO_3$: Phase diagram for $La_{1-x}Ba_xMnO_3$ ($x < 0.33$)," Phys. Rev. B **77**, 064424 (2008).

[19]U. Zammit, S. Paoloni, F. Mercuri, M. Marinelli, and F. Scudieri, "Photopyroelectric calorimeter for the simultaneous thermal, optical, and structural characterization of samples over phase transitions," AIP Adv. **2**, 012135 (2012).

[20]P. Villars and J. L. C. Daams, "Atomic-environment classification of the chemical elements," J. Alloys Compd. **197**, 177–196 (1993).

[21]J. L. Wang, C. Marquina, M. R. Ibarra, and G. H. Wu, "Structure and magnetic properties of RNi_2Mn compounds (R = Tb, Dy, Ho, and Er)," Phys. Rev. B **73**, 094436 (2006).

[22]N. K. Singh, P. Kumar, K. G. Suresh, and A. K. Nigam, "Investigations on magnetic and magnetocaloric properties of the intermetallic compound TbAgAl," J. Appl. Phys. **105**, 023901 (2009).

[23]F. Yuan, J. Du, and B. Shen, "Controllable spin-glass behavior and large magnetocaloric effect in Gd-Ni-Al bulk metallic glasses," Appl. Phys. Lett. **101**, 032405 (2012).

[24]H. Zhang, B. G. Shen, Z. Y. Xu, J. Shen, F. X. Hu, J. R. Sun, and Y. Long, "Large reversible magnetocaloric effects in ErFeSi compound under low magnetic field change around liquid hydrogen temperature," Appl. Phys. Lett. **102**, 092401 (2013).

[25]J. C. Debnath and J. Wang, "Magnetocaloric effect in $HoMn_2Si_2$ compound with multiple magnetic phase transitions," Intermetallics **78**, 50 (2016).

[26]A. Murtaza, W. Zuo, J. Mi, Y. Li, A. Ghani, M. Yaseen, M. Tahir Khan, C. Hao, K. Li, Z. Dai, S. Yang, and Y. Ren, "Magnetocaloric effect and critical exponent analysis around magnetic phase transition in $NdCo_2$ compound," J. Phys. D: Appl. Phys. **53**, 345003 (2020).

[27]H. E. Stanley, *Introduction to Phase Transitions and Critical Phenomena* (Oxford University Press, 1971).

[28]A. K. Pramanik and A. Banerjee, "Critical behavior at paramagnetic to ferromagnetic phase transition in $Pr_{0.5}Sr_{0.5}MnO_3$: A bulk magnetization study," Phys. Rev. B **79**, 214426 (2009).

[29]A. Oleaga, A. Salazar, M. Ciomaga Hatnean, and G. Balakrishnan, "Three-dimensional Ising critical behavior in $R_{0.6}Sr_{0.4}MnO_3$(R = Pr, Nd) manganites," Phys. Rev. B **92**, 024409 (2015).

[30]M. Campostrini, M. Hasenbusch, A. Pelissetto, P. Rossi, and E. Vicari, "Critical exponents and equation of state of the three-dimensional Heisenberg universality class," Phys. Rev. B **65**, 144520 (2002).

[31]M. Campostrini, A. Pelissetto, P. Rossi, E. Vicari, "25-th order high-temperature expansion results for three-dimensional Ising-like systems on the simple-cubic lattice," Phys. Rev. E **65**, 066127 (2002).

[32]B. K. Banerjee, "On a generalized approach to first and second order magnetic transitions," Phys. Lett. **12**, 16–17 (1964).

[33]M. E. Fisher, S.-k. Ma, and B. G. Nickel, "Critical exponents for long-range order interactions," Phys. Rev. Lett. **29**, 917–920 (1972).

[34]A. R. Chowdhury, G. S. Collins, and C. Hohenemser, "Static universality class implied by the critical exponents of Gd," Phys. Rev. **33**, 6231 (1986).

[35]A. Herrero, A. Oleaga, P. Manfrinetti, A. Provino, and A. Salazar, "Critical behavior of the ferromagnetic transition in GdSc(Si,Ge) intermetallic compounds," Intermetallics **101**, 64–71 (2018).

[36]A. Oleaga, A. Herrero, A. Salazar, A. V. Garshev, V. O. Yapaskurt, A. V. Morozkin, "Magnetocaloric properties and unconventional critical behavior in $(Gd,Tb)_6(Fe,Mn)Bi_2$ intermetallics," J. Alloys Compd. **843**, 155937 (2020).

[37]V. Franco, A. Conde, J. M. Romero-Enrique, and J. S. Blázquez, "A universal curve for the magnetocaloric effect: An analysis based on scaling relations," J. Phys.: Condens. Matter **20**, 285207 (2008).

[38]C. Romero-Muñiz, R. Tamura, S. Tanaka, and V. Franco, "Applicability of scaling behavior and power laws in the analysis of the magnetocaloric effect in second-order phase transition materials," Phys. Rev. B **94**, 134401 (2016).
[39]V. Franco, J. S. Blázquez, and A. Conde, "Field dependence of the magnetocaloric effect in materials with a second order phase transition: A master curve for the magnetic entropy change," Appl. Phys. Lett. **89**, 222512 (2006).
[40]V. Franco, A. Conde, V. K. Pecharsky, and K. A. Gschneidner, Jr., "Field dependence of the magnetocaloric effect in Gd and $(Er_{1-x}Dy_x)Al_2$: Does a universal curve exist?," Europhys. Lett. **79**, 47009 (2007).
[41]R. Caballero-Flores, V. Franco, A. Conde, and L. F. Kiss, "Influence of the demagnetizing field on the determination of the magnetocaloric effect from magnetization curves," J. Appl. Phys. **105**, 07A919 (2009).
[42]V. Franco, R. Caballero-Flores, A. Conde, Q. Y. Dong, and H. W. Zhang, "The influence of a minority magnetic phase on the field dependence of the magnetocaloric effect," J. Magn. Magn. Mater. **321**, 1115–1120 (2009).
[43]Y. Su, Y. Sui, J.-G. Cheng, J.-S. Zhou, X. Wang, Y. Wang, and J. B. Goodenough, "Critical behavior of the ferromagnetic perovskites $RTiO_3$ (R = Dy, Ho, Er, Tm, Yb) by magnetocaloric measurements," Phys. Rev. B **87**, 195102 (2013).
[44]L. Li, Y. Yuan, Y. Zhang, R. Pöttgen, and S. Zhou, "Magnetic phase transitions and large magnetic entropy change with a wide temperature span in HoZn," J. Alloys Compd. **643**, 147 (2015).
[45]S. Fujieda, Y. Hasegawa, A. Fujita, and K. Fukamichi, "Thermal transport properties of magnetic refrigerants $La(Fe_xSi_{1-x})_{13}$ and their hydrides, and $Gd_5Si_2Ge_2$ and MnAs," J. Appl. Phys. **95**, 2429–2431 (2004).
[46]A. Salazar, "On thermal diffusivity," Eur. J. Phys. **24**, 351–358 (2003).